Available online at www.sciencedirect.com
ScienceDirect
Journal of the European Ceramic Society 30 (2010) 1803–1808
www.elsevier.com/locate/jeurceramsoc

# A high performance solid oxide fuel cells operating at intermediate temperature with a modified interface between cathode and electrolyte

Baoan Fan [a,*], Jiabao Yan [a], Wenping Shi [b]

[a] *Key Laboratory of Coal Conversion and New Carbon Materials, Hubei Province, Wuhan University of Science and Technology, Wuhan 430081, PR China*

[b] *Institute of Chemical Defense of PLA, Beijing 102205, PR China*

Received 22 March 2009; received in revised form 16 January 2010; accepted 27 January 2010
Available online 21 February 2010

**Abstract**

By adding 1% $Bi_2O_3$ (mol%) into LSCF ($La_{0.54}Sr_{0.44}Co_{0.2}Fe_{0.8}O_{3-\delta}$), a layer of dense LSCF film is introduced to the upside of yttria stabilized zirconia (YSZ) electrolyte. The dense film increases the interface contact area and reduces the interface ion transfer resistance between cathode and electrolyte remarkably. As a result, the cell performance is greatly elevated from 492 to 901 mW cm$^{-2}$ at 650 °C. Besides, on the basis of careful observation of the cathode surface by FE-SEM, the function of $Bi_2O_3$ to promote the cathode sintering is speculated. The $Bi_2O_3$ and the LSCF come into being a kind of eutectic liquid. The eutectic liquid flows down from the cathode bulk to the interface between the cathode and the electrolyte where it accumulates to form a dense layer. This dense layer illuminates the function of adding $Bi_2O_3$ into LSCF cathode.


*Keywords:* Sintering; Interface; Electrical properties; Solid oxide fuel cells; Bismuth oxide

## 1. Introduction

Solid oxide fuel cells (SOFCs) offer a low-pollution technology to generate electricity electrochemically with high efficiency. Recent efforts aimed at decreasing the cost of SOFCs by lowering the operating temperature to 700 °C or less.[1] Decreasing operating temperature can bring several advantages, such as using cheaper materials for interconnects and manifolds, simplifying seal and corrosion problems and elevating lifetime and reliability of SOFCs.[2] Nevertheless, if the operating temperature of SOFCs is reduced, the cell performance will deteriorate for the increase of both ohmic resistance of electrolyte and polarization resistance of electrodes.[3] Therefore, the microstructure and the materials must be optimized for the intermediate temperature solid oxide fuel cells (IT-SOFCs).

So far, significant progresses have been made in this aspect. Some efforts were dedicated to the optimization of electrolyte by reducing the thickness of YSZ to only several microns[4,5] or by applying alternative materials with higher ionic conductivity, such as LSGM[6,7] or doped-ceria.[3,8] Other efforts focused on the optimization of cathode by using the state-of-the-art LSM/YSZ composite materials[2,9] or replacing them with mixed ionic and electronic conductor such as LSCF[10,11] and SSC.[12] In addition, the optimization of anode structure and composition has been also investigated by many researchers.[13,14] However, the optimization of interface between the cathode and the electrolyte was seldom reported.

In this paper, the restrictive factor to the cell performance was detected based on the analysis of cell resistance, which proved that the interface contact resistance between the cathode and the electrolyte is a key factor to the cell performance. By adding little $Bi_2O_3$ into cathode, the interface contact state was improved for the enlargement of contact area, therefore the interface contact resistance was greatly reduced with a result of remarkable increase of cell performance. In addition, the mechanism of adding $Bi_2O_3$ to promote the cathode sintering was discussed on the basis of careful observation of cathode

* Corresponding author at: Mail Box: 144, Wuhan University of Science and Technology, Wuhan 430081, China. Tel.: +86 13297099152; fax: +86 027 86568662.
*E-mail address:* fanbaoan@yahoo.com.cn (B. Fan).

0955-2219/$ – see front matter. 
doi:10.1016/j.jeurceramsoc.2010.01.035

microstructure by field emission scanning electron microscope (FE-SEM).

## 2. Experiments

### 2.1. Powder synthesis

The LSCF powder was synthesized by a citrate complexation (Pechini) route. The AR reagents of lanthanum oxide ($La_2O_3$), strontium carbonate ($SrCO_3$), cobaltous nitrate ($Co(NO_3)_2{\cdot}6H_2O$) and ferric nitrate ($Fe(NO_3)_3{\cdot}9H_2O$) as starting materials were precisely weighed in the composition and the mass of LSCF desired to be synthesized. First, the $La_2O_3$ was dispersed in little deioned water and dissolved by adding concentrated nitric acid ($HNO_3$, 65.0–68.0 wt%) dropwise under churning. Then, the $SrCO_3$ was also dissolved by adding concentrated nitric acid drop by drop so that there is no extra nitric acid remaining. Next, the $Co(NO_3)_2{\cdot}6H_2O$ and $Fe(NO_3)_3{\cdot}9H_2O$ were dissolved in the solution followed by adding citric acid in the molar ratio of 1.5 to all metal ions. Then, the pH value of the solution was adjusted to about 8 by dropping concentrated ammonia solution (25.0–28.0 wt%). Subsequently, the solution was heated to vaporize water until it was turned into a viscous sol. Afterwards the sol was placed in a Muffle oven and fired at 400 °C for 30 min to burn out organic ingredients. When the oven was cooled down to room temperature, the precursor foam was collected for the subsequent baking at 700 °C for 5 h with a heating rate of 10 °C $min^{-1}$.

### 2.2. Cell fabrication

Black nickel oxide powder (NiO, HSG-010-1998, Biyan, Beijing China) and nano-sized 8YSZ powder ($[Y_2O_3]_{0.08}[ZrO_2]_{0.92}$, HWY-N-13.5, Huawang, Guangdong China, $D_{50} = 153$ nm) were used to prepare Ni-8YSZ anode ceramic powder. The powder was made by ball-milling 65 wt% NiO powder and 35 wt% 8YSZ powder at 600 rpm for 12 h with ethanol as a dispersant. After ethanol has been evaporated completely, the anode powder was crushed and then pressed into a disc with a diameter of ~20 mm and a thickness of ~1 mm under uniaxial pressure of 62 MPa. The green anode disc was subsequently calcined at 850 °C for 2 h to strengthen the mechanical property of the anode substrates. A thin layer of 8YSZ electrolyte film was deposited on the one side of the anode substrates by a dip-coating technique.[5] The anode and 8YSZ electrolyte bi-layer framework was then sintered at 1250 °C for 2 h to obtain a dense electrolyte film. After sintering, the thickness of the anode substrates was about 0.8 mm and the diameter of the bi-layer framework was about 16 mm.

The cathode paste was prepared by ball-milling the LSCF powder with terpineol at a solids content of 25% at 800 rpm for 30 h, to which 0.5% ethyl cellulose (EC) as a film-forming agent and 5% additif mouillant et (disperbyk-2050, BYK Chemie, Germany) as a dispersant were added relative to LSCF. In the case of cathode with $Bi_2O_3$, the appropriate amount of precursor $Bi(NO_3)_3$ was first dissolved in acetic acid, followed by mixed with LSCF power in the molar ratio of $Bi_2O_3$:LSCF = 1:100. The paste was subsequently brushed on the electrolyte side of the bi-layer using a screen-printing technique to form a complete cell. Finally, the cell was sintered at 800 °C for 2 h.

### 2.3. Cell test

Cells performance was measured by a lab-made device. The anode chamber was fed in pure hydrogen, while the cathode was exposed to ambient atmosphere. The anode side was sealed by Ag paste and the cathode surface was brushed with Pt paste as current collectors. Two Ag silks were connected to anode and cathode respectively, serving as voltage and current probes. The current–voltage (*I–V*) characteristic curves of the cell were plotted by measuring closed circuit voltage under different steady current densities provided by a potentiostat (DJS-292, Leizi Xinjing, Shanghai, China). The cell power density was calculated by multiplying closed circuit voltage with current density. The electrochemical impedance was measured by an impedance analyzer (PM6306, Fluke, UK) with an excitation potential of 50 mV over a frequency range from 1 MHz to 50 Hz under open circuit state. The microstructure and morphology of cells were observed by FE-SEM (JSM-6700F, JEOL, Japan).

### 2.4. Sample preparation

The sample of cell cross-section for FE-SEM observation was prepared by cutting the cell into two or several tablets using a shear clamp as an instrument. The polished surface of LSCF dense layer between the electrolyte and the cathode was prepared by soaking the cell in 0.5 mol/L hydrochloric acid solution for 220 s to etch away the incompact LSCF cathode grains, then rinsing it with deioned water to remove the remnant hydrochloric acid and drying it at 120 °C for 2 h.

## 3. Results and discussion

Fig. 1 shows the X-ray diffraction (XRD) pattern of $La_{0.54}Sr_{0.44}Co_{0.2}Fe_{0.8}O_{3-\delta}$ after its precursors were calcined at 700 °C for 5 h, which exhibits a well-defined orthorhom-

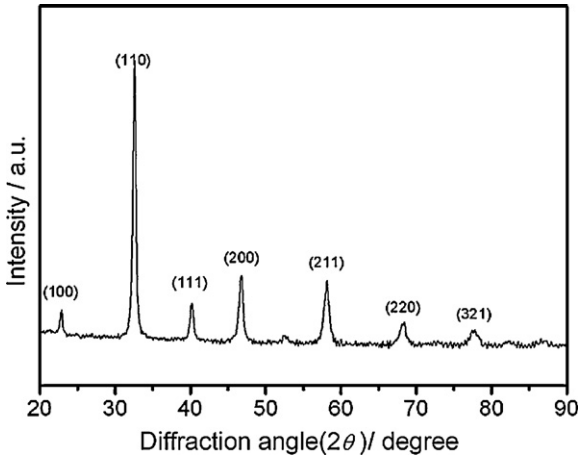


Fig. 1. XRD pattern of $La_{0.54}Sr_{0.44}Co_{0.2}Fe_{0.8}O_{3-\delta}$.

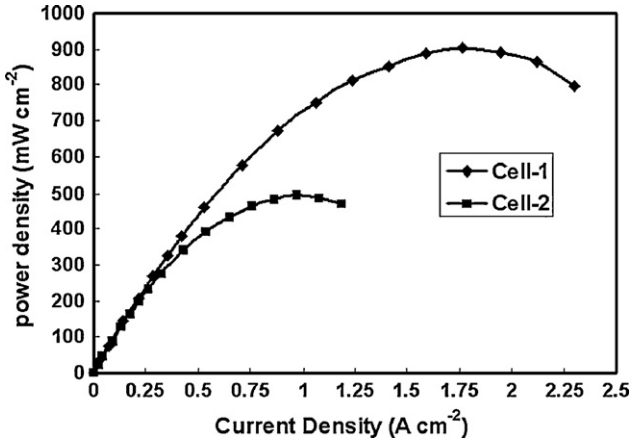


Fig. 2. Electrical performance of the Cell-1 (with $Bi_2O_3$ in cathode) and the Cell-2 (without $Bi_2O_3$ in cathode).

bic perovskite structure without any other peaks suggesting the synthesized LSCF powder with high phase purity.

In order to find the effect of adding bismuth oxide into cathode on cell performance, the cell power densities at different current densities were measured at 650 °C and the results were showed in Fig. 2 (cells added with and without $Bi_2O_3$ in cathode are labeled as the Cell-1 and the Cell-2 respectively). From the figure, it can be found that there is a large improvement of the cell performance for the Cell-1 than the Cell-2. The maximum power density for the Cell-2 only approaches to 492 mW $cm^{-2}$ compared with 901 mW $cm^{-2}$ for the Cell-1.

The reason of electrical performance of the Cell-1 superior to the Cell-2 can be illustrated by their *I–V* curves, which were plotted in Fig. 3. From the figure, it can be found that each curve almost takes on a straight line, indicating cells performance mainly being restricted by the cell ohmic resistance not by the polarization resistance. According to the slope of the straight part of *I–V* curves, the total ohmic resistance can be calculated as 0.28 Ω $cm^2$ for the Cell-1 and 0.50 Ω $cm^2$ for the Cell-2. Therefore, the bigger total ohmic resistance of the

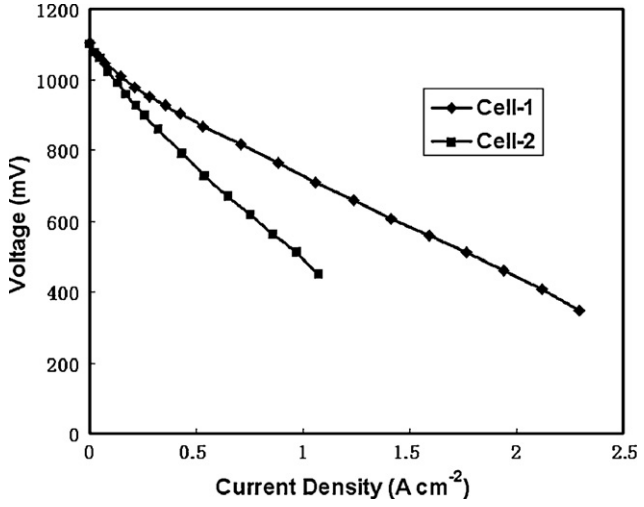


Fig. 3. *I–V* curves of the Cell-1 (with $Bi_2O_3$ in cathode) and the Cell-2 (without $Bi_2O_3$ in cathode) measured at 650 °C.

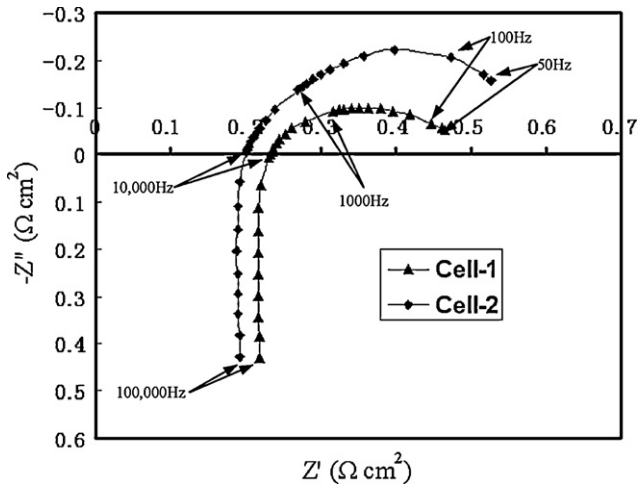


Fig. 4. EIS of the Cell-1 (with $Bi_2O_3$ in cathode) and the Cell-2 (without $Bi_2O_3$ in cathode) measured at 650 °C.

Cell-2 is the extrinsic reason for its poor electrical performance.

For the sake of further investigating the reason why the Cell-2 presents a so high total ohmic resistance, the electrochemical impedance spectrum (EIS) experiments were performed, whose results were plotted in Fig. 4. From the figure, it can be seen that each spectrum takes on a look of a subsiding semicircle with a drooping tail. The intercept of impedance spectrum with the real axis ($Z'' = 0$) at high frequencies represents the resistance of the electrolyte.[15] Accordingly, the electrolyte resistances of 0.23 Ω $cm^2$ for the Cell-1 and 0.20 Ω $cm^2$ for the Cell-2 can be read from Fig. 4. The difference between the total ohmic resistance calculated from the *I–V* curves and the resistance of electrolyte read from the impedance spectra is the interface resistance (i.e. $R_{interface} = R_{total} - R_{electrolyte}$).[16] In this case, the interface resistance of the Cell-1 and the Cell-2 can be easily calculated as 0.05 and 0.3 Ω $cm^2$. Hereto, it can be seen that the intrinsical reason of the Cell-2 exhibiting a poor electrical performance lies in its bigger interface resistance. The interface resistance is composed by the electrolyte/anode interface resistance and electrolyte/cathode interface resistance. Because the two cells have the same anode in this case, the difference of interface resistance only can be attributed to the electrolyte/cathode interface resistance. The interface resistance of electrolyte/cathode includes the resistance of $O^{2-}$ diffusion and charge exchange in the electrode, and the resistance of ion transfer across the cathode/electrolyte interface. The resistance of diffusion and charge exchange of $O^{2-}$ in the electrode depends on the density and mobility of oxygen vacancies in electrode materials.[17] Since the two cells are constructed by the same cathode material, they should exhibit the same $O^{2-}$ exchange and diffusion resistance. The $O^{2-}$ transfer resistance across the cathode/electrolyte interface lies on contact state and contact area between electrolyte and cathode. A sufficient contact between electrolyte and cathode will greatly reduce the interface transfer resistance.

Figs. 5 and 6 show the microstructure photograph of locally magnified cross-section of the Cell-1 and the Cell-2 respectively. From Fig. 5, it can be found that there exists a dense layer

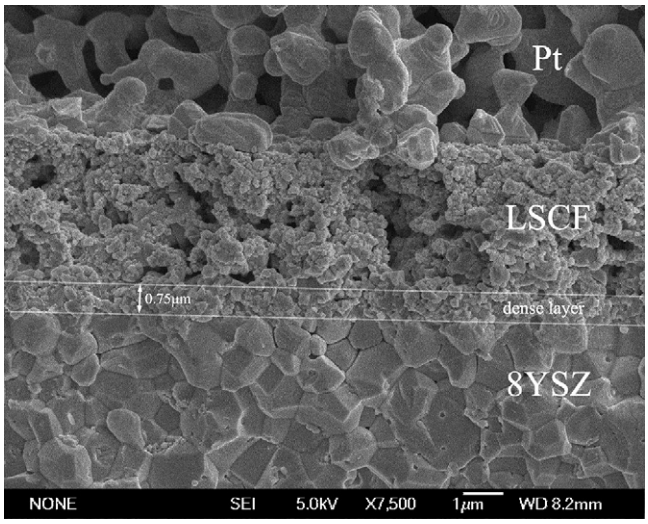


Fig. 5. Locally magnified FE-SEM photograph of the Cell-1 (with $Bi_2O_3$ in cathode) electrolyte/cathode interface.

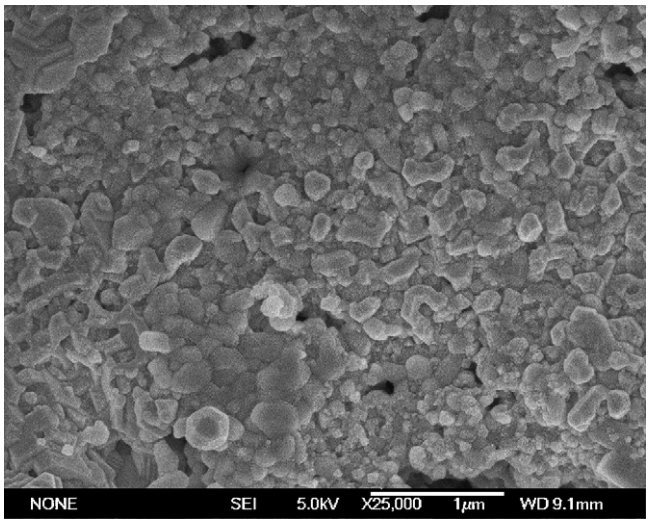


Fig. 7. The surface FE-SEM photograph of dense LSCF layer of the Cell-1 (with $Bi_2O_3$ in cathode) polished by chemical etch.

of LSCF grains between the cathode and the 8YSZ electrolyte with a thickness of about 0.75 μm. Therefore the contact state between the electrolyte and the cathode in the Cell-1 is plane-to-plane. In contrast, from Fig. 6, it can be detected that the cathode grains are dotted on the electrolyte surface. Accordingly the contact state between the electrolyte and the cathode in the Cell-2 is dot-to-plane. In view of this, it can be seen that the insufficient contact state is the main reason of the Cell-2 exhibiting a higher interface resistance than that of the Cell-1.

In order to further testify there exists a layer of compact LSCF grains, the cathode surface was polished by chemical etch and the surface morphology was showed in Fig. 7. From the figure, it can be found that the LSCF layer adjacent to the YSZ electrolyte is almost compacted and there are some traces of grains melting and sintering, which would be induced by the additive $Bi_2O_3$ in cathode.

For the purpose of investigating the effect of $Bi_2O_3$ on promoting the cathode sintering, the cathode powder added with $Bi_2O_3$ was prepared by drying the cathode slurry including $Bi(NO_3)_3$ at 120 °C and then firing it at 350 °C to burn out the organic solvent and decompose the $Bi(NO_3)_3$ into $Bi_2O_3$. Subsequently the cathode powder was pressed into a disc under the pressure of 274 MPa followed by calcined at 800 °C for 2 h. Then the top-surface and undersurface of the disc were observed by FE-SEM, just showed in Figs. 9 and 10 respectively. In parallel, the cathode powder without $Bi_2O_3$ was also processed in the same way. Fig. 8 shows the surface FE-SEM photograph of cathode disc without $Bi_2O_3$. From the figure, it can be seen that although there are some sintering phenomena between adjacent cathode grains to some extent, the grains still keep their original configuration and sharp boundary. On the contrary, from Fig. 9, it can be seen that the LSCF grains are partly sintered together and the neck-bottle phenomena are very clear. The boundary of

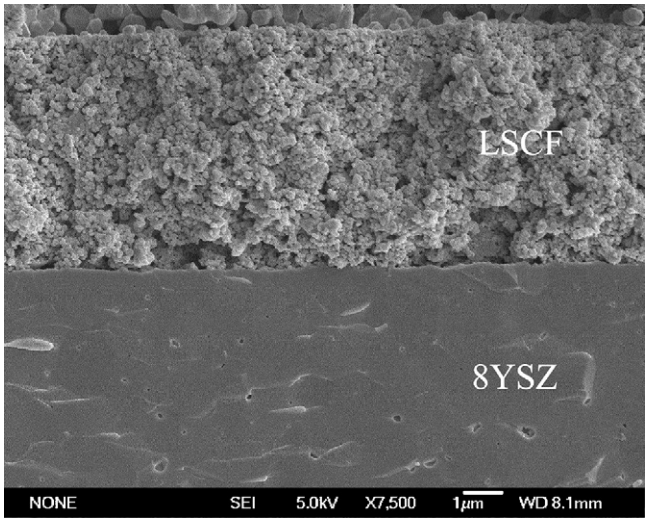


Fig. 6. Locally magnified FE-SEM photograph of the Cell-2 (without $Bi_2O_3$ in cathode) electrolyte/cathode interface.

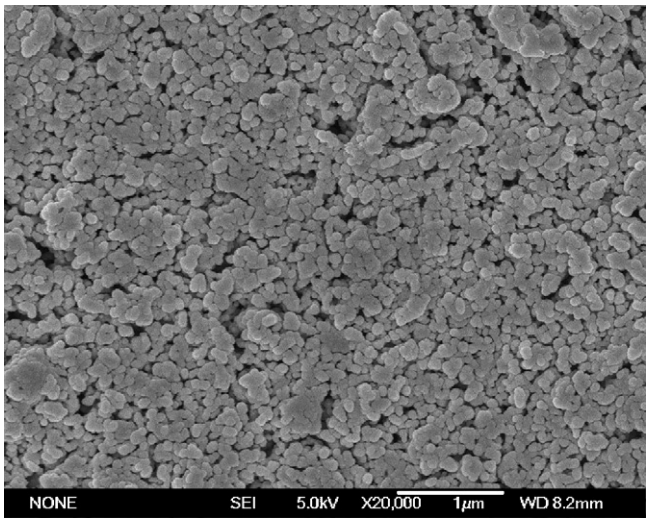


Fig. 8. The FE-SEM photograph of cathode disc surface without $Bi_2O_3$.

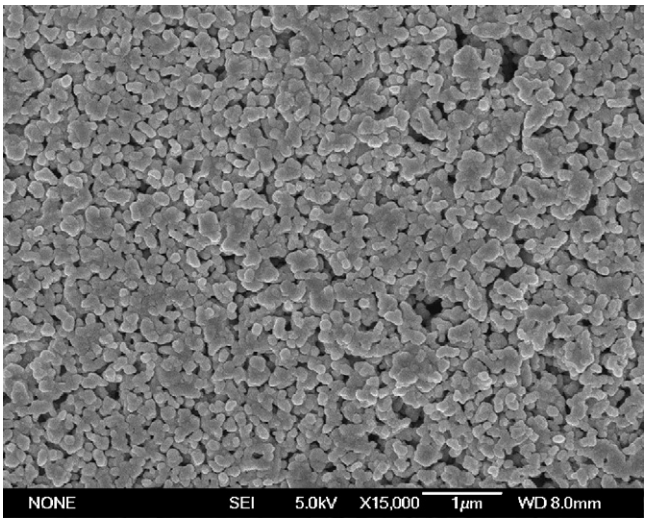


Fig. 9. Top-surface FE-SEM photograph of cathode disc with $Bi_2O_3$.

grain becomes obscure and the agglomerate grains are sintered together, but the appearance of cathode disc still keeps a porous structure.

Furthermore, from Fig. 10 it can be found that almost all cathode grains have grown together and the cathode disc almost fully compacted. By careful observation, it can be found that there are some traces of liquid melting and flowing, indicating that the liquid-phase sintering is the predominant sinter mechanism induced by $Bi_2O_3$.

On the basis of these observations, we can figure out that the function of $Bi_2O_3$ in promotion of cathode sintering is followed. Because the $Bi_2O_3$ has a very lower melting point (about 825 °C[18]) and a similar phase structure with LSCF, it would be very prone to form a kind of eutectic mixture with LSCF. During the sintering process, the eutectic mixture melts and flows down from the cathode bulk until to the electrolyte surface under the function of gravity, for the gravity is the only force whose direction is downward (capillary force is isotropy and internal stress is outward). Since the 8YSZ electrolyte has been compacted, the eutectic liquid cannot flow any more only to accumulate on the upside of the electrolyte to form a dense layer of LSCF. Therefore the contact state between the cathode and the electrolyte is transformed from dot-to-plane into plane-to-plane, which induces the interface contact resistance being reduced greatly.

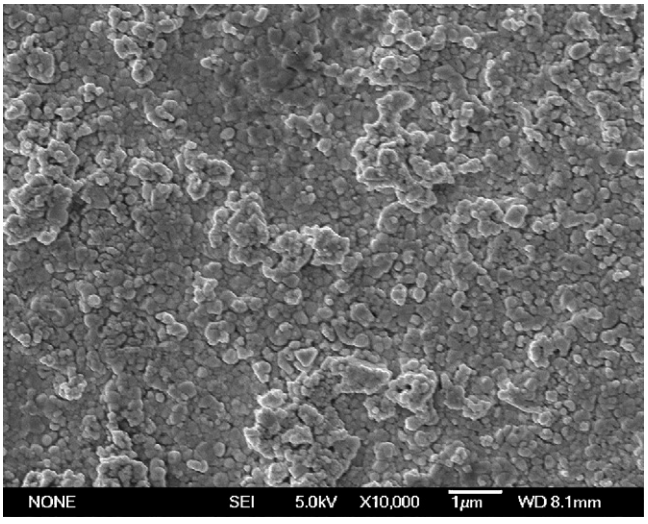


Fig. 10. Undersurface FE-SEM photograph of cathode disc with $Bi_2O_3$.

In order to testify the eutectic liquid does flow down to the electrode/electrolyte interface, another experiment was preformed. The LSCF cathode power added with $Bi_2O_3$ was pressed into a strong disc under above pressure. The disk was placed between two alumina flakes. Then the sandwich consisted by LSCF disc and two alumina flakes was sent to Muffle oven and sintered at 800 °C for 5 h. After the oven was cooled down to room temperature, the sandwich was taken out to find the bottom alumina flake sticking to the LSCF disk, while the top alumina flake is very easily separated from the LSCF disk. This experiment confirms the melting eutectic does flow down under the drive of gravity force.

Steele and Bae[19] also reported that introducing a thin layer of dense cathode adjacent to the electrolyte by electrostatic spray assisted vapor deposition (ESAVD) can reduce the interface contact resistance.

## 4. Conclusions

By comparing the difference of the total ohmic resistance and the electrolyte resistance, it can be found that the definitively restrictive factor to the cell performance is the interface contact resistance of electrolyte/cathode in this case. During cathode sintering, as the electrolyte has been densified and cannot shrink any more, the cathode grains do not tightly be sintered on the electrolyte surface, which induces the increase of interface contact resistance between the cathode and the electrolyte with a result of cell performance deterioration. By adding little $Bi_2O_3$ into cathode as sintering additive to promote the cathode sintering, a thin layer of dense LSCF grains formed on the electrolyte surface. Just for this dense layer of LSCF grains, the interface contact resistance is greatly reduced and the cell performance is elevated from 492 to 901 mW $cm^{-2}$ at 650 °C. Besides, the mechanism of $Bi_2O_3$ as a sintering additive was speculated based on the observations of microstructure evolution of the cathode, which is pointed to liquid-phase sintering. The $Bi_2O_3$ and the LSCF come into being a kind of eutectic liquid. The eutectic liquid flows down from the cathode bulk to the electrolyte surface under the function of gravity where it accumulates to form a dense layer. This dense layer of LSCF grains brings about the decrease of the contact resistance at cathode/electrolyte interface and the improvement of cell performance.

## Acknowledgements

We would like to express our gratitude for financial support from Wuhan University of Science and Technology and for intellectual backing of my tutor Qingshan Zhu.

## References


1. Liu Y, Zha S, Liu M. Nanocomposite electrodes fabricated by a particle-solution spraying process for low-temperature SOFCs. *Chem Mater* 2004;**16**:3502–6.
2. Haanappel VAC, Mertens J, Rutenbeck D, Tropartz C, Herzhof W, Sebold D, et al. Optimisation of processing and microstructural parameters of LSM cathodes to improve the electrochemical performance of anode-supported SOFCs. *J Power Sources* 2005;**141**:216–26.
3. Leng YJ, Chan SH, Jiang SP, Khor KA. Low-temperature SOFC with thin film GDC electrolyte prepared in situ by solid-state reaction. *Solid State Ionics* 2004;**170**:9–15.
4. Sprio S, Guicciardi S, Bellosi A, Pezzotti G. Yttria-stabilized zirconia films grown by radiofrequency magnetron sputtering: structure, properties and residual stresses. *Surf Coat Technol* 2006;**200**:4579–85.
5. Zhang Y, Gao J, Peng D, Meng G, Liu X. Dip-coating thin yttria-stabilized zirconia films for solid oxide fuel cell applications. *Ceram Int* 2004;**30**:1049–53.
6. Huang K, Goodenough JB. A solid oxide fuel cell based on Sr- and Mg-doped $LaGaO_3$ electrolyte: the role of a rare-earth oxide buffer. *J Alloy Compd* 2000;**303–304**:454–64.
7. Fukui T, Ohara S, Murata K, Yoshida H, Miura K, Inagaki T. Performance of intermediate temperature solid oxide fuel cells with $La(Sr)Ga(Mg)O_3$ electrolyte film. *J Power Sources* 2002;**106**:142–5.
8. Matsui T, Inaba M, Mineshige A, Ogumi Z. Electrochemical properties of ceria-based oxides for use in intermediate-temperature SOFCs. *Solid State Ionics* 2005;**176**:647–54.
9. Xu X, Xia C, Xiao G, Peng D. Fabrication and performance of functionally graded cathodes for IT-SOFCs based on doped ceria electrolytes. *Solid State Ionics* 2005;**176**:1513–20.
10. Hwang HJ, Moon JW, Lee S, Lee EA. Electrochemical performance of LSCF-based composite cathodes for intermediate temperature SOFCs. *J Power Sources* 2005;**145**:243–8.
11. Mai A, Haanappel VAC, Uhlenbruck S, Tietz F, Stöver D. Ferrite-based perovskites as cathode materials for anode-supported solid oxide fuel cells. Part I. Variation of composition. *Solid State Ionics* 2005;**176**:1341–50.
12. Xia C, Rauch W, Chen F, Liu M. $Sm_{0.5}Sr_{0.5}CoO_3$ cathodes for low-temperature SOFCs. *Solid State Ionics* 2002;**149**:11–9.
13. Wang FH, Guo RS, Wei QT, Zhou Y, Li HL, Li SL. Preparation and properties of Ni/YSZ anode by coating precipitation method. *Mater Lett* 2004;**58**:3079–83.
14. Lee CH, Lee HY, Seung M. Microstructure and anodic properties of Ni/YSZ cermets in solid oxide fuel cells. *Solid State Ionics* 1997;**98**:39–48.
15. Xia C, Liu M. Microstructures, conductivities, and electrochemical properties of $Ce_{0.9}Gd_{0.1}O_2$ and GDC–Ni anodes for low-temperature SOFCs. *Solid State Ionics* 2002;**152-153**:423–30.
16. Ji Y, Liu J, He T, Cong L, Wang J, Su W. Single intermedium-temperature SOFC prepared by glycine–nitrate process. *J Alloy Compd* 2003;**353**:257–62.
17. Fan B, Liu X. A-deficit LSCF for intermediate temperature solid oxide fuel cells [J]. *Solid State Ionics* 2009;**180**:973–7.
18. Sammes NM, Tompsett GA, Näfe H, Aldinger F. Bismuth based oxide electrolytes-structure and ionic conductivity. *J Eur Ceram Soc* 1999;**19**:1801–26.
19. Steele BCH, Bae JM. Properties of $La_{0.6}Sr_{0.4}Co_{0.2}Fe_{0.8}O_{3-x}$ (LSCF) double layer cathodes on gadolinium-doped cerium oxide (CGO) electrolytes. II. Role of oxygen exchange and diffusion. *Solid State Ionics* 1998;**106**:255–61.